Facile kinetics of Li-ion intake causes superior rate capability in MWCNT@TiO_2 nanocomposite battery anodes.

Próspero Acevedo-Peña[†], *Marta Haro*[‡], *Marina E. Rincón*[†], *Juan Bisquert*[‡]

*and Germà Garcia-Belmonte**[,‡]

[†]Instituto de Energías Renovables, Universidad Nacional Autónoma de México, 62580 Temixco, Mexico

[‡]Photovoltaics and Optoelectronic Devices Group, Departament de Física, Universitat Jaume I, 12071 Castelló, Spain

Corresponding Author

Germà Garcia-Belmonte, e-mail: garciag@fca.uji.es, tel.: +34 964 397548.

Published: *Journal of Power Sources,* 268 (2014) 397-403

Highlights:

- TiO_2 and MWCNT@TiO_2 would potentially exhibit comparable specific capacity.
- Outstanding rate capability of the coated nanotubes is observed compared to TiO_2.
- MWCNT provides electrons through the Ti-C bond thereby assisting Li^+ ion intake.

Graphical Abstract:

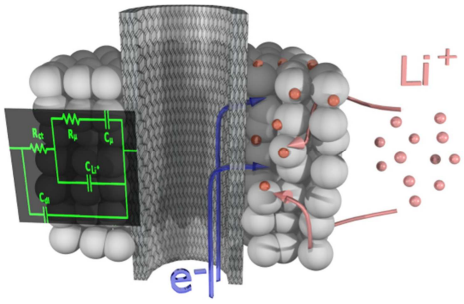

Abstract. Nanotechnology produces hybrids with superior properties than its individual constituents. Here MWCNT@TiO_2 composites have been synthesized by controlled hydrolysis of titanium isopropoxide over MWCNT, to be incorporated into Li-ion battery electrodes. Outstanding rate capability of the coated nanotubes is observed in comparison to pristine TiO_2. Specific storage capacity as high as 250 mAh g^{-1} is achieved for the nanocomposite electrode which doubles that encountered for TiO_2-based anodes. The mechanism explaining the enhancement in power performance has been revealed by means of electrochemical impedance methods. Although both pristine TiO_2 and MWCNT@TiO_2 would potentially exhibit comparable specific capacity, the charge transfer resistance for the latter is reduced by a factor 10, implying a key role of MWCNTs to favor the interfacial Li^+ ion intake from the electrolyte. MWCNT efficiently provides electrons to the nanostructure through the Ti-C bond which assists the Li^+ ion incorporation. These findings provide access to the detailed lithiation kinetics of a broad class of nanocomposites for battery applications.

Keywords. Li-ion batteries, Core-shell materials, Carbon nanotubes, TiO_2, Electrode kinetics, Electrochemical impedance spectroscopy.

1. Introduction

Li-ion batteries are considered as the most prominent energy storage technology to be used in diverse applications such as portable electronic devices and electric and hybrid vehicles, due to its high specific capacity, low weight, and durability [1, 2]. However, most of the likely materials to be employed as electrodes in these cells are limited by low Li^+ diffusion, scarce electron transport, and high resistances at the electrode/electrolyte interfaces when the charge and discharge cycle is carried at high rates. In order to improve the power performance of the batteries, different approaches have been adopted to develop materials with superior transport of electrons as well as Li^+ ions [2, 3]. The use of nanostructured materials has been widely explored to diminish the pathway for Li^+ ion transport during the charging-discharging cycles in the cell and to alleviate mechanical stress. Particularly, 1D-structures have shown outstanding performances as they provide a directional path for electrons transport toward the current collector, and a high surface area for Li^+ ion insertion, shortening the path for Li^+ ion diffusion [4, 5].

Combining different materials allows to create composites with superior properties than its raw constituents, bringing together the best properties of each component in order to enhance its functionality. Obtained composite materials based on carbon nanotubes and TiO_2 have exhibited good results for this particular application, due to the improvement in the electronic transport

offered by the carbon, the reversibility for Li^+ ion insertion and mechanical stability provided by the TiO_2 [4-6]. Additionally, these composites have shown better rate capability during cycling that is one of the mayor disadvantages of the pristine TiO_2 due to its low electronic conductivity [6-11]. Despite the evident connection between electron availability and high power performance, the exact mechanism responsible for the enhanced rate capability is still unclear. Most of the electrochemical characterization of this composite has been carried out by using direct current techniques, obtaining information only of the overall electrochemical performance of the material, which provides little understanding of different steps involved during the charging-discharging process of the electrodes.

Recently, we have proposed a model to study the lithiation kinetic through equivalent circuit analysis of the experimentally obtained electrochemical impedance spectroscopy (EIS) spectra [12, 13]. This approach facilitates the extraction of resistances involved in the overall lithium ion storage, as well as the insertion-extraction process occurring during the cycling of the battery. Herein, it was synthesized MWCNT@TiO_2 nanocomposites with superior rate capability than pristine TiO_2, and the interaction between MWCNT and TiO_2 in MWCNT@TiO_2 anodes during the charging-discharging process was studied with EIS in order to understand the specific role played by each material. We observe that the high electron conductivity of MWCNT renders the charge transfer resistance accounting for the intake of Li^+ ions from the solution to extremely low values, independently of the electrode potential. On the contrary, pristine TiO_2 anodes exhibit a current limitation originated by high charge transfer resistances that severely reduces power performance. The results obtained might be extrapolated to the family of core-shell materials based on carbon nanotubes that recently have attracted much attention for developing efficient lithium-ion battery materials [6, 14-16].

2. Experimental

MWCNTs were synthesized by spray pyrolysis of a mixture of 0.2M ferrocene (Aldrich, 98 %) + turpentine oil (70 % α-pinene, 18 % β-pinene), following the procedure reported elsewhere [4]. The core-shell composite of MWCNT@TiO_2 was obtained by controlled hydrolysis of titanium isopropoxide over the MWCNT as follows: *i*) 20mg of MWCNT were suspended in 60mL of 2-propanol in an ultrasonic bath, *ii*) 600µL of titanium isoproxide was added to the suspension and kept it during 30 min in the ultrasonic bath, *iii*) the suspension was transferred into a volumetric flask with continuous stirring, and 600µL of Millipore water dissolved in 20mL of iso-propanol was added drop by drop into the suspension, and *iv*) the suspension was heated at boiling point during 6h keeping the stirring and using a reflux system to avoid the change in the solvent volume. In order to obtain the pristine TiO_2 it was carried the same procedure but missing the step *i*). Finally, the obtained suspensions were filtered, dried at 120°C during 2h and heat treated at 400°C during 4h to obtain the polymorph anatase in the TiO_2. The obtained materials were characterized by TEM using a JEM-2010F FASTEM, and by Raman Spectroscopy using a Thermo Scientific DXR Raman microscope.

The electrochemical characterization was carried out using a two-electrodes Swagelok cell with metallic lithium as both the counter and the reference electrode. The working electrode was prepared by mixingthe active material (e.g. MWCNT, TiO_2 and MWCNT@TiO_2)with carbon black and poly(vinylidenedifluoride) in a 85:10:5 weight ration, respectively. The electrolyte used was 1.0 M $LiPF_6$ in a 50:50 (w/w) mixture of ethylene carbonate and diethyl carbonate, and a glass fiber (Grade GF/C260µm-thick) from Whatman was used as a separator. Cell assembly was carried out in an N_2-filled glovebox. Electrochemical characterization was performed using

a PGSTAT-30 potentiostat from Autolab equipped with an impedance module. 1C was defined as 168 mA $g^{-1}$for the charge-discharge tests [5].

3. Results and discussion

3.1 Structural characterization

TEM images of the synthesized materials are shown in Fig. 1. The MWCNT (Fig. 1a) shows an external diameter among 40-90 nm, with the presence of ferrous impurities in the inner part of the nanotubes formed during the synthesis that were not leached during its functionalization with concentrated HNO_3. Moreover, the TiO_2 synthesized in absence of MWCNT is composed by crystals around 10 nm of diameter as observed in Fig. 1b. When the titanium isopropoxide was hydrolyzed over the MWCNT a core-shell structure was obtained, with a TiO_2 shell thickness of around 100 nm (Fig. 1c-d). The morphology of the TiO_2 crystal in the MWCNT@TiO_2 seems to be the same to that of the pristine TiO_2.

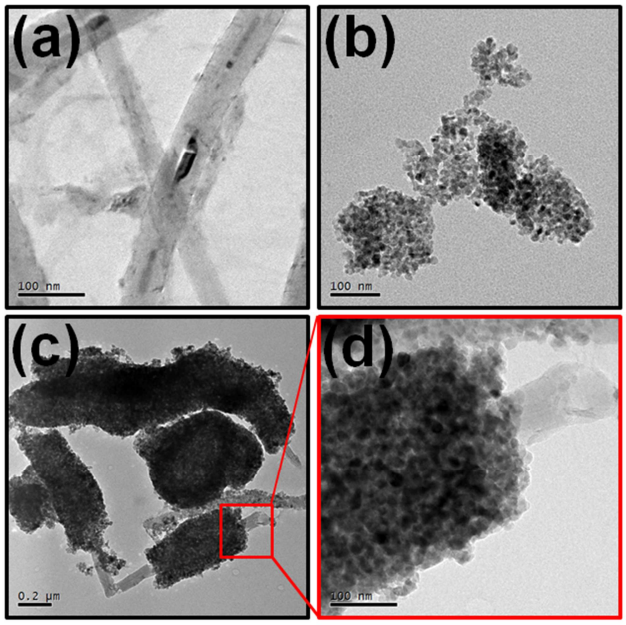

Figure 1. TEM images of (a) MWCNT, (b) TiO_2 anatase and (c and d) MWCNT@TiO_2 nanocomposite material.

The Raman spectra for the synthesized materials are shown in Fig. 2. MWCNT@TiO_2 exhibits the five characteristics peaks for anatase as well as the D, G and 2D bands characteristic for the carbon nanotubes [9]. When the TiO_2 is grown over the MWCNT a change in the shape and Raman shift is provoked in the anatase peaks compare to that of the pristine TiO_2, this variations can be associated either with the interaction between the TiO_2 and MWCNT or to the formation of structural defects such as oxygen vacancies or, less probably, carbon doping during the heat treatment [17]. XRD spectra for the MWCNT, TiO_2 and MWCNT@TiO_2 materials were measured informing that crystallite size of the anatase is not altered by adding the MWCNT during the synthesis (see Supporting Information). Then, the blue shift in the $E_{1g}(1)$ vibration mode seems to be related to the strain in the TiO_2 caused by the interface MWCNT/TiO_2. Additionally, in the MWCNT@TiO_2 composite two vibrational modes related to Ti-C bond were

detected at 265 cm^{-1} and 420 cm^{-1} [18], evidencing the formation of Ti-C bond in the core-shell interface during the synthesis of the composite. The presence of these defects will surely affect the Ti^{4+}/Ti^{3+} reaction during Li^{+} ion insertion, however, little is known on this topic. On the other hand, the shape of the G-band for the MWCNT confirms its metallic nature which is required to improve the electronic transport of the composite [8, 9, 19]. The ratio of the D and G band is slightly altered when the TiO_2 is forming a shell around the MWCNT probably due to an increase in the disorder caused by Ti-C bonds in the interface. Then the formation of Ti-C bonds might have a determinant role in the charge transfer enhancement (see below).

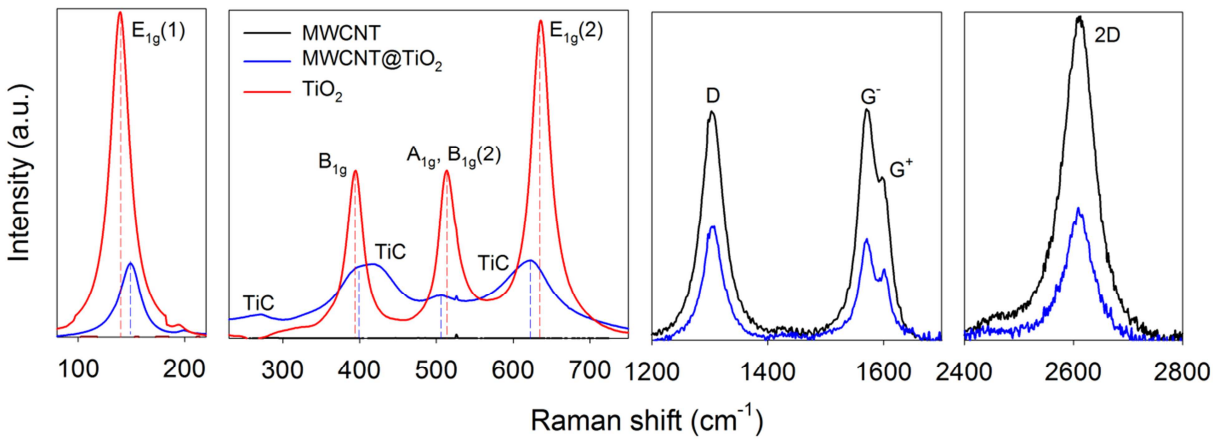

Figure 2. Raman spectra of the materials studied. The Raman spectra are divided in different section in which are shown the principal vibration modes of the materials.

3.2 Electrochemical response

The voltammetric characterization of the TiO_2 and MWCNT@TiO_2 is shown in the Fig. 3. The faradaic processes related to the Li^{+} ion insertion and extraction from the TiO_2 lattice were detected in a similar potential window for the TiO_2 and MWCNT@TiO_2, with a higher potential difference between both processes for the former. Additionally, the Li^{+} ion insertion and

extraction in the TiO_2 exhibit two broader peaks, compared with the narrow peaks shown by the MWCNT@TiO_2. It is worth mentioning that the anodic peak related to the Li^+ ion extraction decays with the cycling for the TiO_2 pristine, meanwhile it remains almost constant for the MWCNT@TiO_2.

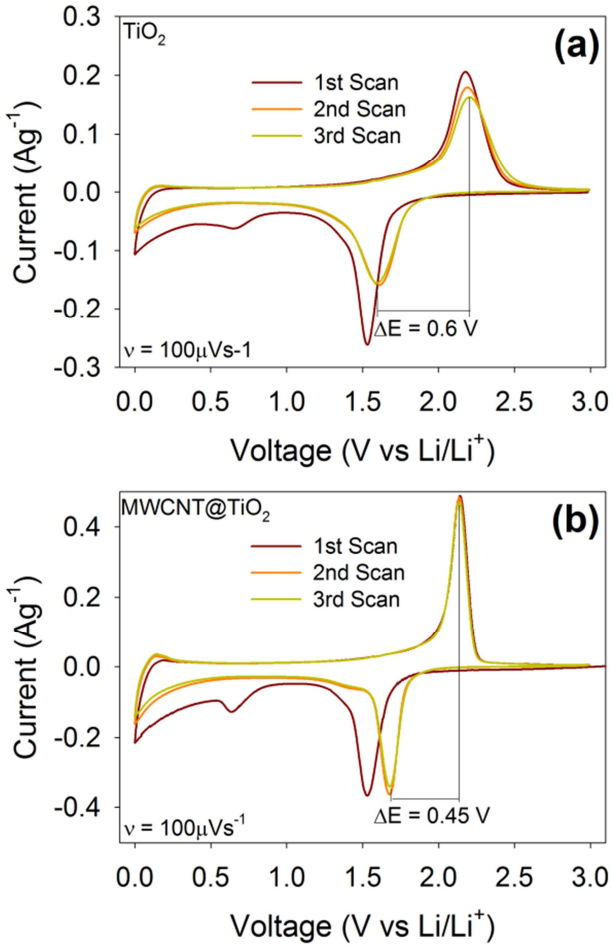

Figure 3. Voltammetric characterization (scan rate = 100μVs^{-1}) of the (a) TiO_2 and (b) MWCNT@TiO_2.

In Fig. 4a-b is shown the third cycle of the charge-discharge curves obtained at different rates for the TiO_2 pristine (a) and the MWCNT@TiO_2 (b). Herein reported pristine TiO_2 has low capacity compared to other crystallographic and morphologic TiO_2 electrodes [20, 21] but close to the

theoretical gravimetric capacity of anatase nanoparticles (165 mAh g^{-1}). In the first charge the measured capacity is 123 $mAhg^{-1}$, although decrease to 100 $mAhg^{-1}$ in the third cycle (figure 4 a) at charge rate of C/10. The lower capacity can be ascribed to the size of the synthesized TiO_2 that has strong influence on both the capacity and reversibility of the electrode [22]. MWCNT@TiO_2 shows higher capacities at every charging-discharging rate with an outstanding better rate capability in comparison with pristine TiO_2. Additionally, the charge and discharge potentials are closer for the MWCNT@TiO_2 at lower rates, with a large plateau for both processes centered at ca. 1.6 V, behavior that has been previously reported for this material [8, 10, 11]. Fig. 4c shows the effect of the cycle number and the charging-discharging rate over the capacity of the anode. Pristine TiO_2 rapidly shows a shrink in the specific capacity with cycle number, vanishing its capacity at 1C, meanwhile MWCNT@TiO_2 remain almost constant at low rates with capacity values around 250 $mAhg^{-1}$, and maintaining a capacity of ~180$mAhg^{-1}$even at 1C. The excellent reversibility of MWCNT@TiO_2 electrode in the range of 1-3 V is also important to avoid the degradation of the electrolyte (reduction phenomena occurs at voltages lower than 1 V) and the necessity of a passivation layer at the electrode/electrolyte interface [20].

In order to discern if an additional amount of carbon-based material, as that introduced with MWCNT, could be the origin of the enhanced capacity and rate kinetics, electrodes comprising 11.8% more CB content were analyzed (see Supporting Information). It is confirmed that the improvement in the performance of the MWCT@TiO_2 is due to the presence of MWCNT and to the core-shell morphology, and no to a merely increase in the quantity of conductive material present in the electrode

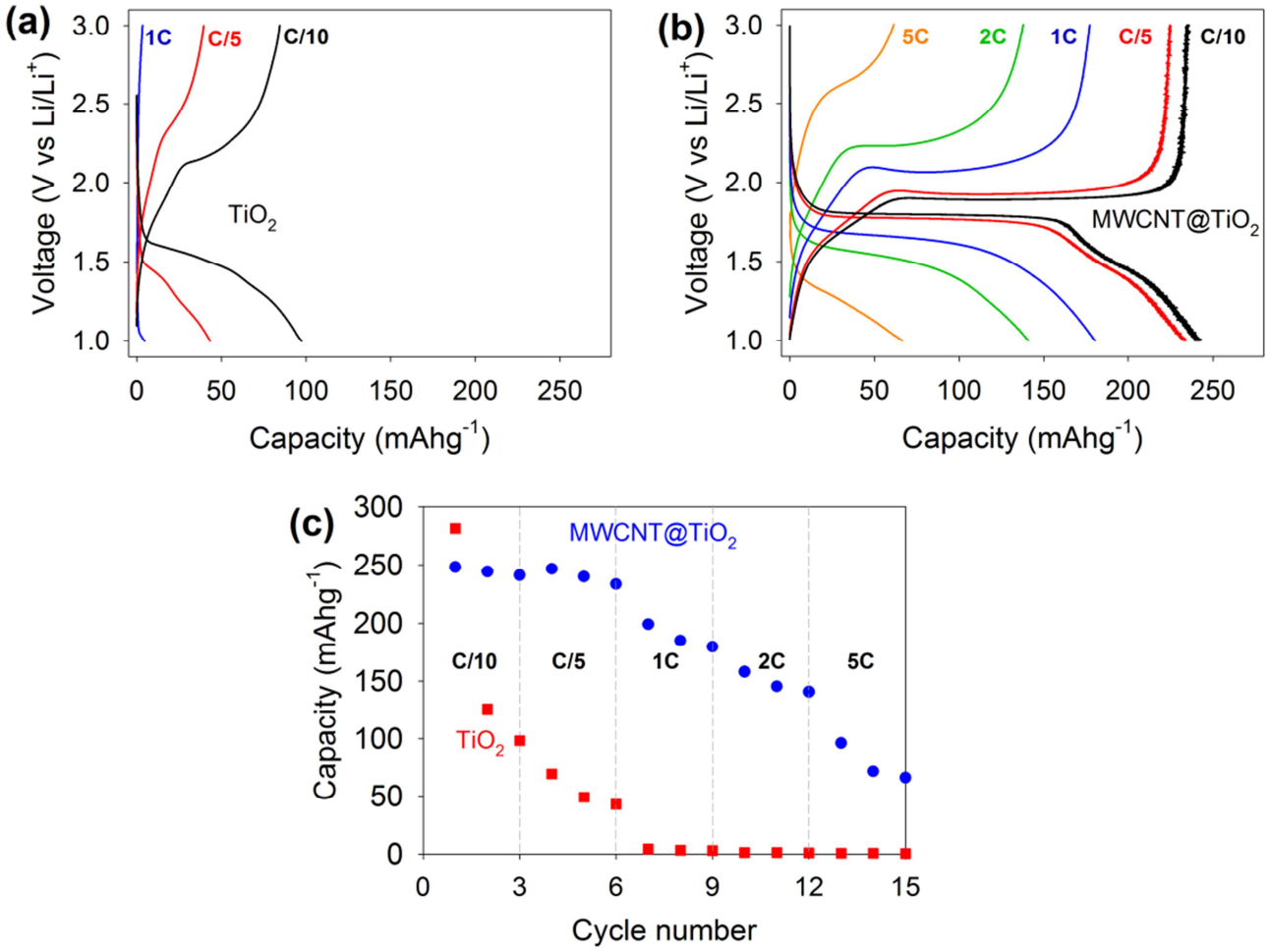

Figure 4. Charge-Discharge curves (third cycle) at different rates for (a) TiO_2 and (b) MWCNT@TiO_2, and effect of cycle number and charge rate over the charge capacity for the TiO_2 and MWCNT@TiO_2 anodes.

3.3 Electrochemical impedance spectroscopy

Aiming at uncovering the origin for the superior rate capability exhibited by MWCNT@TiO_2anodes, the assembled half batteries were characterized by means of electrochemical impedance spectroscopy to discern the different steps involved in the charge-discharge process. EIS measurements were carried in the potential window between 0.5

V and 3.0 V vs Li/Li^+. In the same way than CV and charge-discharge characterization, the EIS measurements were carried first charging the anode and then dischanging it at a very low rate to ensure the steady state, measuring the EIS spectra potentiostatically at different stages of the Li^+ ion insertion and extraction. Figure 5 shows as example three different Nyquist diagrams experimentally obtained during the charging (a, c and e) and discharging process (b, d and f). In this study, MWCNT were included as a blank and to support the discussion derived from these results.

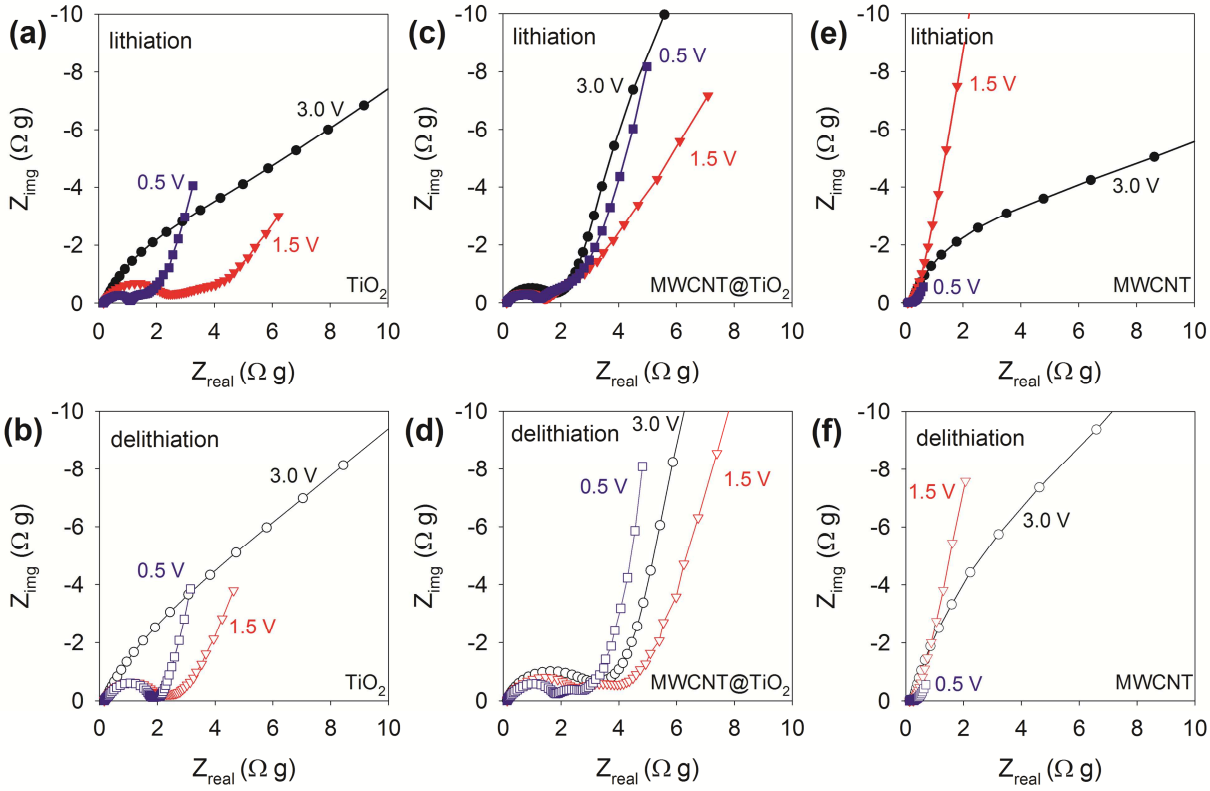

Figure 5. Nyquist diagrams experimentally measured at different stages of charge (a, c and e) and discharge (b, d and f) for: (a and b) TiO_2, (c and d) MWCNT@TiO_2, and (e and f) MWCNT.

All the Nyquist spectra exhibit two patterns with distinguishable time constants associated to specific electrochemical mechanisms.At high frequencies a flattened arc is formed related to the interfacial charge transfer resistance R_{ct} in parallel with the double layer capacitance C_{dl}. These are processes occurring at the interface between the hybrid nanostructure and the electrolyte. At low frequencies the electrodes show a capacitive behavior associated with the Li^+ ion storage inside the material which is manifested by its chemical capacitance C_μ [23]. This capacitance relates to the differential change in electrode charge upon voltage variation and it is connected to the ability of the oxide matrix to react with Li^+ ions. In fact it is a slow-rate version of the cyclic voltammetry experiment, and strictly corresponds to the derivative of the charge-discharge curve as $C_\mu = -dQ/dV$ in the case of extremely slow (quasi-equilibrium) rate. For intercalation compounds the diffusion of Li^+ ion inside the active matrix significantly contributes to the rate-limiting mechanisms. In those materials an intermediate frequency resistance arises from the transport of Li^+ ion before reaching stable sites within the matrix [24]. More recently this resistance has been connected to the electrochemical lithiation reaction forming in this specific case Li_xTiO_2 [12, 13]. It is worth mentioning that for TiO_2 at high voltage for charging and discharging, the charge transfer resistance is so high that it does not allow detecting other processes in the frequency range employed in the characterization as observed in Fig. 5a-b.These considerations suggest a simple equivalent circuit which accounts for the high-frequency response by means of R_{ct} and C_{dl}, and models the low-frequency part using a series combination of resistive R_{lr} (lithiation reaction) and capacitive (chemical) C_μ elements. An additional capacitive element C_{Li^+} accounts for the contribution of inserted Li^+ before lithiation reaction is accomplished to form Li_xTiO_2 [12]. This capacitance accounts for the intermediate-frequency arc of the impedance plots in Fig. 5. Figure 6 shows the proposed equivalent circuit, along with a

schematic representation of the MWCNT-provided electrons to assist Li^+ ion intake from the electrolyte.

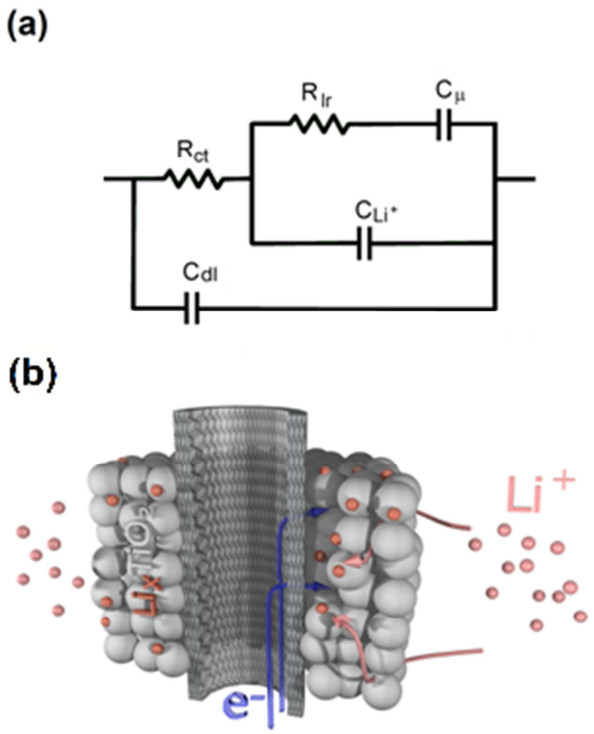

Figure 6. (a) Equivalent circuit showing the principal electrochemical mechanisms: charge transfer resistance R_{ct}, double layer capacitance C_{dl}, chemical capacitance C_{μ}, Li^+ capacitance C_{Li^+}, and lithiation-reaction resistance, $R_{lr.}$. (b) Scheme of the Li^+ insertion mechanism into the TiO_2 that is favored by electron conduction through MWCNT. Carbon nanaotubes efficiently provide electrons to the oxide, allowing for a detriment in the interfacial charge transfer resistance.

.

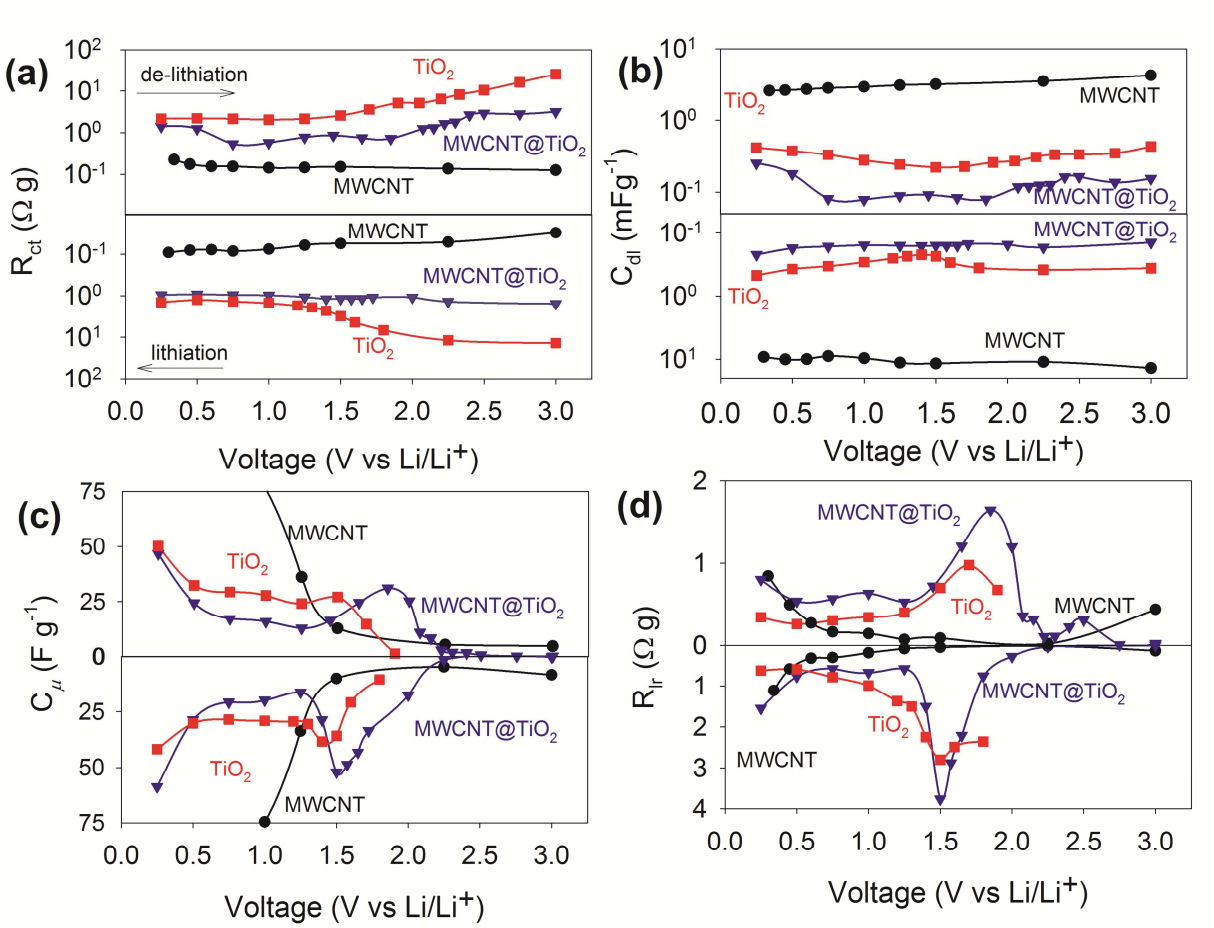

Figure 7. The main parameters derived from fitting of EIS data: (a) Charge transfer resistance, R_{ct}, (b) double layer capacitance, C_{dl}, (c) charge capacitance, C_{μ}, and (d) lithiation-reaction resistance, R_{lr}.

Main parameters extracted from fitting using the equivalent circuit in Fig.6a are summarized in Fig.7. Experiments were performed both during charge and discharge in potentiostatic mode. The high-frequency elements R_{ct} and C_{dl} (Fig.7a-b) exhibit rather voltage-independent values for electrodes comprising MWCNT, with and without TiO_2. Interestingly, the lower R_{ct} is observed when only MWCNTs are checked (~0.1 Ω g). The deposition of TiO_2 shell increases R_{ct} in

approximately one order of magnitude (~1 Ω g). This fact allows connecting this last resistance to the process of lithium intake from the solution to the TiO_2 solid matrix (see Fig. 6b), and not to the electron transport in MWCNTs. Pristine TiO_2 presents a much larger charge transfer resistance for potentials in excess of 1.5 V (~10 Ω g). Compared to MWCNT@TiO_2, which keeps it at ~1 Ω g, this is a huge increment. At lower potentials both TiO_2 and MWCNT@TiO_2 are able to insert Li^+ ions with similar (diminished) hindrance. It has been observed for other insertion compounds that R_{ct} is directly related to the electronic conductivity of the host material [25]. High conductive hosts facilitate the Li^+ ion to overcome the potential barrier appearing at the electrolyte/semiconductor interface. It should be stressed here the role of MWCNTs to assist the Li^+ ion incorporation into the TiO_2 matrix. MWCNTs not only assure the presence of electrons needed to complete the lithiation reaction, but also are able to favor the Li^+ ion intake by enhancing the TiO_2 electron availability through the formation of Ti-C bonds. The nanostructure then simultaneously fulfills the two basic requirements that a battery electrode should offer: enhanced electron conductivity of the lithiation compound and large surface area to foster Li^+ incorporation. This is the main mechanism that explains the superior rate capability (power performance) observed in Fig. 3c of MWCNT@TiO_2 in comparison to TiO_2 electrodes.

Since the interfacial charge transfer resistance is not the only current-limiting element, it is also necessary to explore the behavior of the low-frequency circuit elements. The chemical capacitance C_μ in Fig. 7c exhibits well-defined peaks both for MWCNT@TiO_2 and TiO_2 electrodes in the lithiation-reaction voltage interval. By examining Fig. 7c one can observe C_μ comparable values around 25-50 Fg^{-1} for both MWCNT@TiO_2 and TiO_2 electrodes. A voltage shift approximately equal to 0.2 V is observed that situates the MWCNT@TiO_2 composite

lithiation reaction peaks at slightly higher potentials, presumably because of the interaction between Ti and C atoms as observed in Raman spectra of Fig. 2. Despite the voltage offset C_μ peaks reach comparable heights that reveal a similar storage capacity at quasi-equilibrium conditions for both MWCNT@TiO_2 and TiO_2 electrodes. The resistance accompanying the lithiation reaction R_{lr} exhibits also a similar behavior giving values of 1-3 Ω g. (Fig. 7d). Differences of a factor two are observed in R_{lr} between MWCNT@TiO_2 and TiO_2 electrodes probably related to the strain in TiO_2 particles caused by the interface MWCNT/TiO_2, which slightly modifies the lithiation reaction kinetics. This reinforces our previous claim connecting the superior MWCNT@TiO_2 rate capability to the lower values observed for the interfacial charge transfer resistance of Fig. 7a.

4. Conclusions

In summary, by separating kinetic and thermodynamics components of the lithiation process, we have shown that the inclusion of MWCNT is beneficial for an extreme enhancement of the rate capability of Li^+ uptake and release in TiO_2. Although both pristine TiO_2 and MWCNT@TiO_2 would potentially exhibit comparable specific capacity, MWCNTs favor the interfacial Li^+ ion intake from the solution by reducing the inherent charge transfer resistance. MWCNT efficiently provides electrons to the nanostructure through the formation of Ti-C bonds, then effectively assisting Li^+ ion incorporation. We also highlight the excellent reversibility of MWCNT@TiO_2 electrode in the range of 1-3 V which is important to avoid the degradation of the electrolyte (reduction phenomena occurs at voltages lower than 1 V). Well-designed core-shell composites are then promising structures to fulfill both energy and power requirements of storage systems.

Acknowledgments

This work has been given the financial support from CONACyT (Project CB-2008/105655) and UNAM (PAPIIT-UNAM IN106912).P. Acevedo-Peña is grateful to UNAM for the Postdoctoral grant and the program CYTED-Nanoenergías. The authors thank to Ph.D. J.C. Calva from IER-UNAM for its help in MWCNT synthesis and to Ph.D. M.G. Almazan from CIDETEQ for its help in Raman spectroscopy characterization. We acknowledge financial support from GeneralitatValenciana (ISIC/ 2012/008 Institute of Nanotechnologies for Clean Energies).

References

[1] Z.-S. Wu, G. Zhou, L.-C. Yin, W. Ren, F. Li, H.-M. Cheng, Nano Energy, 1 (2012) 107-131.
[2] M. Reddy, G. Subba Rao, B. Chowdari, Chem. Rev., 113 (2013) 5364-5457.
[3] S. Goriparti, E. Miele, F. De Angelis, E. Di Fabrizio, R. Proietti Zaccaria, C. Capiglia, J. Power Sources, (2014).
[4] F.-F. Cao, Y.-G. Guo, S.-F. Zheng, X.-L. Wu, L.-Y. Jiang, R.-R. Bi, L.-J. Wan, J. Maier, Chem. Mater., 22 (2010) 1908-1914.
[5] S. Ding, J.S. Chen, Adv. Funct. Mater., 21 (2011) 4120-4125.
[6] H. Zhou, L. Liu, X. Wang, F. Liang, S. Bao, D. Lv, Y. Tang, D. Jia, Journal of Materials Chemistry A, 1 (2013) 8525-8528.
[7] T. Song, H. Han, H. Choi, J.W. Lee, H. Park, S. Lee, W.I. Park, S. Kim, L. Liu, U. Paik, Nano Reserch, accepted (2014).
[8] B. Wang, H. Xin, X. Li, J. Cheng, G. Yang, F. Nie, Scientific Reports, 4 (2014) 3729.
[9] K. Hemalatha, A. Prakash, K. Guruprakash, M. Jayakumar, Journal of Materials Chemistry A, 2 (2014) 1757-1766.
[10] Z. Wen, S. Ci, S. Mao, S. Cui, Z. He, J. Chen, Nanoscale Research Letters, 8 (2013) 499.
[11] M.N. Hyder, B.M. Gallant, N.J. Shah, Y. Shao-Horn, P.T. Hammond, Nano Lett., 13 (2013) 4610-4619.
[12] C. Xu, Y. Zeng, X. Rui, J. Zhu, H. Tan, A. Guerrero, J. Toribio, J. Bisquert, G. Garcia-Belmonte, Q. Yan, J. Phys. Chem. C, 117 (2013) 17462−17469.
[13] F. Martinez-Julian, A. Guerrero, M. Haro, J. Bisquert, D. Bresser, E. Paillard, S. Passerini, G. Garcia-Belmonte, J. Phys. Chem. C, 118 (2014) 6069−6076.
[14] R. Bhandavat, G. Singh, ACS applied materials & interfaces, 4 (2012) 5092-5097.
[15] R. Bhandavat, G. Singh, The Journal of Physical Chemistry C, 117 (2013) 11899-11905.
[16] G. Qin, S. Xue, Q. Ma, C. Wang, CrystEngComm, 16 (2014) 260-269.
[17] Q. Wu, Q. Zheng, R. van de Krol, The Journal of Physical Chemistry C, 116 (2012) 7219-7226.
[18] V. Kiran, S. Sampath, Nanoscale, 5 (2013) 10646-10652.

[19] J.H. Lehman, M. Terrones, E. Mansfield, K.E. Hurst, V. Meunier, Carbon, 49 (2011) 2581-2602.
[20] A.R. Armstrong, G. Armstrong, J. Canales, R. García, P.G. Bruce, Adv. Mater., 17 (2005) 862-865.
[21] Y.S. Hu, L. Kienle, Y.G. Guo, J. Maier, Adv. Mater., 18 (2006) 1421-1426.
[22] Y.G. Guo, Y.S. Hu, W. Sigle, J. Maier, Adv. Mater., 19 (2007) 2087-2091.
[23] J. Bisquert, Phys. Chem. Chem. Phys., 5 (2003) 5360-5364.
[24] J. Song, M.Z. Bazant, J. Electrochem. Soc., 160 (2013) A15-A24.
[25] R. Hass, J. Garcia-Cañadas, G. Garcia-Belmonte, J. Electroanal. Chem., 577 (2005) 99–105.